ASTRONOMY & ASTROPHYSICS
SUPPLEMENT SERIES

*Astron. Astrophys. Suppl. Ser.* **126,** 3-13 (1997)



# CO and HI in a southern sample of interacting galaxies⋆

## I. The data

**C. Horellou and R. Booth**

Onsala Space Observatory, Chalmers University of Technology, S-439 92 Onsala, Sweden
e-mail: horellou@oso.chalmers.se, roy@oso.chalmers.se

Received January 6; accepted February 3, 1997

**Abstract.** Using SEST, the Parkes antenna and the Australia Telescope Compact Array, we have made a survey of the $^{12}$CO(1−0) and HI emission of an optically-selected sample of ≈ 60 southern interacting and merging galaxies. In this paper we present the data and determine global masses of neutral gas (in molecular and atomic form) for the observed galaxies. We have detected HI in 26 systems and found that these galaxies have less than 15% of their gas in molecular form.

**Key words:** galaxies: interaction — galaxies: ISM — galaxies — evolution — radio lines: galaxies

### 1. Introduction

Observations at many wavelengths have revealed the important rôle of interstellar gas in the evolution of systems of interacting galaxies. Being highly dissipative, the gas reacts irreversibly to perturbations. It is generally believed that it looses its angular momentum and is driven towards the central region of the galaxy because of the gravitational torques produced by the interaction. Atomic gas (HI) from the outer parts sweeps in, is converted into the molecular phase ($H_2$), and forms new stars. Powerful starbursts and nuclear activity can be triggered in one or both of the colliders, giving rise to enhanced H$\alpha$, far-infrared and radiocontinuum emission (e.g., Kennicutt et al. 1987; Xu & Sulentic 1991; Hummel et al. 1990). Strongly interacting galaxies also have enhanced CO emission which suggests that a larger supply of molecular gas is available for star-formation (e.g., Braine & Combes 1993).

Observations of infrared-luminous galaxies have revealed an HI deficiency (e.g., Martin et al. 1991). However, the existence of such a conversion from HI gas into $H_2$ is far from being established for less infrared-luminous objects since most work to date has focused on the extreme examples (through far-IR selection) rather than on the interactions themselves. Indeed, not all interacting galaxies are luminous in the far-infrared, and studies of unbiased samples of interacting galaxies are necessary to clarify the relation between dynamics, gas content and induced star-formation.

A complete sample of interacting galaxies does exist in the literature. It has been compiled by Bergvall (1981) and contains all interacting galaxies in a well-defined region of the Southern sky with a blue magnitude lower than 14.5 (see below). In contrast to most existing samples, the galaxies in the Bergvall sample have not been selected on their far-infrared emission. The optical and near-infrared properties of this sample have been studied (Johansson & Bergvall 1990; Bergvall & Johansson 1995, hereafter JB90 and BJ95). Our work has been to add to the extensive existing database, where possible, information about the neutral gas content of these galaxies by observing the two main transitions of atomic and molecular gas: HI at $\lambda$ 21 cm and the $J = 1-0$ rotational line of the CO molecule at $\lambda$ 2.6 mm.

In the following we present the sample and the already existing datasets. We show the $^{12}$CO(1−0) and HI spectra along with optical images of the galaxies and list the parameters of the CO and HI lines as well as the derived molecular and atomic gas masses. The molecular gas masses $M(H_2)$ have been computed from the $^{12}$CO(1−0) line intensities using a standard conversion factor established for our own galaxy (Strong et al. 1988). The use of this conversion factor may be meaningful only for massive galaxies such as the Milky Way. This is discussed in Sect. 4.3. The analysis of the data and a study of the relationship between gas content and star-formation indicators will be presented in a forthcoming paper.

*Send offprint requests to*: C. Horellou

⋆ Figure 3 in its entirely is only available in electronic form at CDS via anonymous ftp to cdsarc.u-strasbg.fr (130.79.128.5) or via http://cdsweb.u-strasbg.fr/Abstract.html

## 2. The sample

### *2.1. Fifty-eight objects in a selected region of the sky*

The sample contains 58 systems of galaxies, numbered from 1 to 59 (the galaxies numbered 57 and 58 are in gravitational interaction and part of the same system). The 58 sample objects come from a catalogue of southern interacting galaxies originally compiled by Bergvall (1981, hereafter B81). The sample contains all interacting galaxies in a limited region of the sky and is complete down to the blue magnitude $m_B < 14.5$. The selection criteria are described in JB90. The surveyed area was limited by $b \leq -30°$ and $\delta \leq -37.5°$. Two types of objects were considered:

i) Interacting galaxies were included in B81 if the diameter of the largest component was $\geq 42''$. Galaxy pairs were regarded as interacting if one of the following criteria was satisfied:

- Both galaxies show a distorted morphology, have an angular separation $\leq$ 6 times the diameter of the largest component and a magnitude difference $\leq 2^{\rm m}$.
- At least one galaxy shows a distorted morphology, and the members have an angular separation $\leq$ twice the diameter of the largest component and a magnitude difference $\leq 3^{\rm m}$.
- The galaxies are physically connected via a well-defined bridge.

ii) Single distorted galaxies were included if the diameter $\geq 1'$.

The sources names, coordinates and some of their characteristics are listed in Table 1, arranged as follows:

- *Column 1*: Galaxy number adapted from Johansson & Bergvall (1990).

- *Column 2*: Number in the ESO catalogue and other names.

- *Columns 3 and 4*: Source coordinates taken from the NED database. Unless specified differently, the positional accuracy is better than 8 arcsec in both coordinates.

- *Column 5*: Radio velocity computed from the heliocentric velocity taken from the NED database or given by Bergvall (private communication).

- *Column 6*: Morphological type taken from the Third Reference Catalogue of Bright Galaxies (de Vaucouleurs et al. 1991, RC3).

- *Column 7*: Decimal logarithm of the isophotal major diameter, $D_{25}$, at 25 mag/arcsec$^2$ taken from the RC3. The unit of $D_{25}$ is 0.1 arcmin.

### *2.2. Distances and luminosities*

Figure 1 shows an histogram of the radial velocities for the sample galaxies (H$\alpha$ was detected by BJ95 in 57 of the 58 galaxy systems). The median velocity is 6903 km s$^{-1}$. All the velocities quoted in this article are heliocentric, using the radio definition $v_{\rm rad} = -c\Delta\nu/\nu$. The distances correspond to a Hubble constant $H_0 = 75$ km s$^{-1}$ Mpc$^{-1}$ ($D = v_{\rm rad}/H_0$).

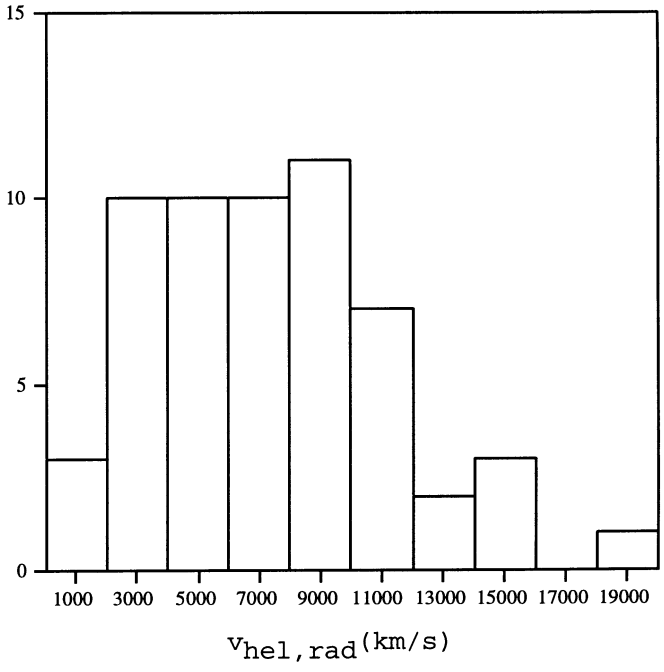


**Fig. 1.** Histogram of the radial velocities (in radio convention) for the sample galaxies

## 3. The existing datasets

In addition to IRAS data, broadband optical and near-infrared photometry ($UBVRIJHK$), broadband images (Cousins $B$ and $V$ and Gunn $i$) and optical spectra are available (JB90 and BJ95).

Blue and $H$-band magnitudes as well as far-infrared parameters of the sample galaxies are listed in Table 2, arranged as follows:

- *Column 1*: Galaxy number adapted from Johansson & Bergvall (1990).

- *Columns 2 and 3*: $H$-band magnitudes, taken from JB90 and blue magnitudes $B_{\rm T}^0$ taken from the RC3.

- *Columns 4 to 7*: IRAS spectral flux densities at 12.5, 25, 60 and 100 $\mu$m, in Jy as given in the NED database.

- *Column 8*: The dust temperature $T_{\rm FIR}$ has been derived from $f_{60}$ and $f_{100}$ by fitting a black body and assuming that the dust emissivity is proportional to $\lambda^{-1}$.

- *Column 9*: The far-infrared luminosities have been computed for the $40 - 120\,\mu$m range using the relation given Lonsdale et al. (1985): $L_{\rm FIR}/L_\odot = 3.94\,10^5\,(D/1\ {\rm Mpc})^2\,(2.58 f_{60} + f_{100})$ where $f_{60}$ and $f_{100}$ are the spectral flux densities at 60 and 100 $\mu$m measured in Jy by IRAS; $D = v_{\rm rad}/75$ (velocities in the radio convention).

*Far-infrared fluxes*: Thirty-eight galaxies of the sample have been detected by IRAS both at 60 and 100 $\mu$m, three

**Table 1.** Galaxy characteristics

| Name | ESO nber, other names | $\alpha$(1950) h m s | $\delta$(1950) $^\circ$ $'$ $''$ | $v_{\rm hel,rad}$ km s$^{-1}$ | Morph. Type | log $D_{25}$ $D_{25}$ in 0.1$'$ |
|---|---|---|---|---|---|---|
| JB01[a] | 193−G 19 | 00 02 56.8 | −50 32 54 | 9489 | .SXT5?P | 1.29 |
| JB02 | 112−IG 08 | 00 31 04.0 | −61 34 18 | 9840 | | |
| JB03_1 | 079−IG 13 NED01 | 00 54 45.3 | −63 45 20 | 10464 | | |
| JB03_2 | 079−IG 13 NED02 | 00 54 50.0 | −63 45 06 | 10255 | .SAR5P. | 0.95 |
| JB04 | 243−G 15, NGC 0322 | 00 54 52.0 | −43 59 48 | 6929 | .L..?P/ | 1.05 |
| JB05 | 079−G 16 | 01 02 32.0 | −64 23 24 | 5916 | .S?.... | 1.03 |
| JB06_1 | 151−IG 36, NGC 0454 NED01 | 01 12 17.0 | −55 39 54 | 3587 | .P..... | 1.26 |
| JB06_2[b] | 151−IG 36, NGC 0454 NED02 | 01 12 23.0 | −55 39 32 | 3587 | | |
| JB07_1 | 244−G 12 NED01 | 01 15 56.0 | −44 43 36 | 6554 | .S..3*P | 1.04 |
| JB07_2 | 244−G 12 NED02 | 01 15 56.0 | −44 43 18 | 6554 | | |
| JB08 | 244−G 17 | 01 18 08.0 | −44 23 24 | 6885 | RSBR1P* | 1.07 |
| JB09 | 244−IG 30 | 01 27 41.0 | −42 34 54 | 7418 | .P..... | 1.05 |
| JB10_1 | 297−G 11, NGC 0633 | 01 34 11.0 | −37 34 42 | 5061 | .SBR3*. | 1.11 |
| JB10_2 | 297−G 12 | 01 34 11.0 | −37 35 48 | 5278 | | |
| JB11_1 | 080−G 02, NGC 0646 NED01 | 01 35 46.0 | −65 09 00 | 8010 | .SXS5P* | 1.11 |
| JB11_2 | 080−G 02, NGC 0646 NED02 | 01 35 55.0 | −65 09 04 | | | |
| JB12_1 | 244−G 46 | 01 36 55.0 | −43 37 18 | 6160 | .L...P. | 0.60 |
| JB12_2 | 244−G 47 | 01 36 59.4 | −43 36 47 | | .L...P. | 1.08 |
| JB13 | 245−G 10 | 01 54 42.0 | −44 13 00 | 5606 | .S..3P. | 1.38 |
| JB14_1 | 299−IG 01 NED01 | 02 23 15.0 | −40 39 36 | 6074 | | |
| JB14_2[c] | 299−IG 01 NED02 | 02 23 14.0 | −40 39 12 | 11364 | | |
| JB15 | 199−G 01 | 02 47 23.0 | −50 08 48 | 8986 | | |
| JB16 | 200−IG 31, NGC 1356 | 03 29 11.0 | −50 28 42 | 11136 | .SXR4P* | 1.14 |
| JB17_1 | 249−IG 31, NGC 1487 NED01 | 03 54 05.0 | −42 30 42 | 815 | .P..... | 1.52 |
| JB17_2 | 249−IG 31, NGC 1487 NED02 | 03 54 05.0 | −42 30 54 | 878 | | |
| JB18 | 117−G 16 | 03 55 55.0 | −60 34 12 | 9046 | .S?.... | 1.20 |
| JB19 | 157−IG 05, NGC 1536 | 04 09 57.0 | −56 36 54 | 1583 | .SBS5P* | 1.30 |
| JB20 | 303−G 17, IC2068 | 04 24 59.0 | −42 12 12 | 4424 | PSAT0*. | 1.09 |
| JB21 | 157−IG 50 | 04 39 33.0 | −52 51 06 | 3592 | .S.4*P/ | 1.22 |
| JB22 | 085−IG 05 | 04 47 49.0 | −63 33 00 | 5983 | | |
| JB23 | 306−G 12 | 05 35 46.0 | −42 28 18 | 10559 | .S?.... | 1.10 |
| JB24 | 205−G 01, NGC 2101 | 05 45 15.0 | −52 06 24 | 1199 | .IBS9P. | 1.29 |
| JB25 | 143−G 04 | 20 00 41.0 | −57 49 18 | 14487 | PSXT4P* | 0.95 |
| JB26 | 105−G 26, McLeish's Object | 20 04 45.0 | −66 21 48 | 10974 | | |
| JB27 | 284−G 28, NGC 6875 | 20 09 40.0 | −46 18 42 | 3088 | .LXS-P* | 1.37 |
| JB28_1 | 073−IG 32, NGC 6872 | 20 11 42.0 | −70 55 18 | 4486 | .SBS3P. | 1.78 |
| JB28_2 | 073−IG 33, IC 4970 | 20 11 44.0 | −70 54 12 | 4641 | .LA.-P* | 0.83 |
| JB29_1[d] | 284-IG 41 NED01 | 20 12 50.0 | −44 27 18 | 5233 | .P..... | 1.10 |
| JB29_2 | 284−IG 41 NED02 | 20 12 51.0 | −44 27 30 | 5157 | | |
| JB30 | 284−IG 45 | 20 13 16.0 | −46 41 12 | 5264 | | 1.25 |
| JB31 | 284−IG 48 | 20 13 46.0 | −45 56 24 | 5283 | | |
| JB32 | 186−G 29, NGC 6889 | 20 15 03.0 | −54 06 48 | 2532 | .SB.4?P | 1.23 |
| JB33[e] | 285- G 04, NGC 6902A | 20 19 33.0 | −44 26 00 | 15774 | .SBS9P. | 1.13 |
| JB34 | 340−G 29 | 20 22 45.0 | −41 05 42 | 9057 | .SB?... | 0.96 |
| JB35_1 | 285−G 19 NED01 | 20 26 09.0 | −42 40 18 | | | |
| JB35_2 | 285−G 19 NED02 | 20 26 10.0 | −42 40 18 | | | |

(a) JB01: uncertainty in position = 30 × 30 arcsec. NED gives also a radio velocity of 10079 km s$^{-1}$.
(b) JB06_2: uncertainty in position = 30 × 30 arcsec.
(c) JB14_2: other authors give $v_{\rm hel,opt}$ = 6321 km s$^{-1}$.
(d) JB29_1: uncertainty in position = 30 × 30 arcsec.
(e) JB33: uncertainty in position = 9 × 9 arcsec.

**Table 1.** continued

| Name | ESO nber, other names | $\alpha$(1950) h m s | $\delta$(1950) ° ′ ″ | $v_{\rm hel,rad}$ km s$^{-1}$ | Morph. Type | log $D_{25}$ $D_{25}$ in 0.1′ |
|---|---|---|---|---|---|---|
| JB36 | 285−IG 35 | 20 31 14.0 | −44 00 48 | 8726 | .P..... | 1.10 |
| JB37 | 341−IG 04 | 20 38 00.0 | −38 22 24 | 5937 | .L..+*P | 1.28 |
| JB38_1 | 187−IG 13 NED01 | 20 41 07.0 | −52 59 36 | 12643 | | |
| JB39_1 | 235−G 23 NED01 | 20 55 03.0 | −49 28 42 | 6756 | .LB?... | 1.20 |
| JB39_2 | 235−G 23 NED02 | 20 55 05.0 | −49 29 30 | | | |
| JB40$^{(f)}$ | 286−IG 19 | 20 55 08.6 | −42 50 36 | 12312 | | 0.88 |
| JB41 | 342−IG 13 | 21 06 51.0 | −37 42 24 | 2733 | .P..... | 1.21 |
| JB42 | 145−G 07, IC 5110 | 21 26 58.0 | −60 13 18 | 8416 | | 1.15 |
| JB43_1 | 236−IG 19 NED01 | 21 28 57.0 | −48 26 00 | 8983 | | |
| JB43_2 | 236−IG 19 NED02 | 21 28 59.0 | −48 25 36 | 9006 | | |
| JB44 | 287−G 40 | 21 34 12.0 | −47 15 36 | 9027 | RSXR4P* | 1.07 |
| JB45_1 | 188−IG 18 NED01 | 21 39 40.0 | −52 55 00 | 5126 | .L..0P. | 1.07 |
| JB45_2 | 188−IG 18 NED02 | 21 39 35.0 | −52 54 36 | 5204 | | |
| JB46_1 | 145−IG 21 NED01 | 21 47 33.0 | −61 26 06 | 18650 | | |
| JB46_2 | 145−IG 21 NED02 | 21 47 36.0 | −61 26 42 | | | |
| JB47 | 288−G 32 | 21 58 33.0 | −42 40 48 | 7826 | PSBS2.. | 0.99 |
| JB48 | 108−IG 18 | 22 08 43.0 | −62 58 18 | 8205 | | 0.84 |
| JB49 | 344−G 13, IC 5174 | 22 09 47.0 | −38 25 12 | 10724 | .SBS3P. | 1.32 |
| JB50 | 108−IG 21 | 22 11 36.0 | −65 48 00 | 3161 | | 1.17 |
| JB51 | 146−G 18, IC 5190 | 22 15 37.0 | −60 08 00 | 7820 | .SBS4P. | 1.10 |
| JB52_1 | 109−IG 22, IC 5250A NED01 | 22 44 00.0 | −65 19 18 | 3090 | .L?.... | 1.47 |
| JB52_2 | 109−IG 22, IC 5250B NED02 | 22 44 05.0 | −65 19 12 | 3179 | | |
| JB53 | 290−G 45, NGC 7476 | 23 02 22.0 | −43 22 06 | 2923 | PSBR2*. | 1.14 |
| JB54 | 240−G 01 | 23 19 05.0 | −48 12 42 | 14555 | | |
| JB55 | 148−IG 10, NGC 7650 GPair | 23 22 31.0 | −58 03 54 | 3140 | .SBS6P* | 1.14 |
| JB56$^{(g)}$ | 240−G 10 | 23 35 03.0 | −47 46 54 | 3161 | .LX.0*P | 1.60 |
| JB57 | 110−G 22, NGC 7733 | 23 39 47.0 | −66 14 06 | 9863 | PSBT3P. | 1.13 |
| JB58 | 110−G 23, NGC 7734 | 23 39 57.0 | −66 13 18 | 10222 | PSBR3P* | 1.15 |
| JB59 | 293−G 22 | 23 55 27.0 | −41 48 36 | 6903 | .L?.... | 0.98 |

(f) JB40: uncertainty in position = 5 × 5 arcsec
(g) HI line at $v_{\rm rad}$ = 2600 km s$^{-1}$ towards JB56.

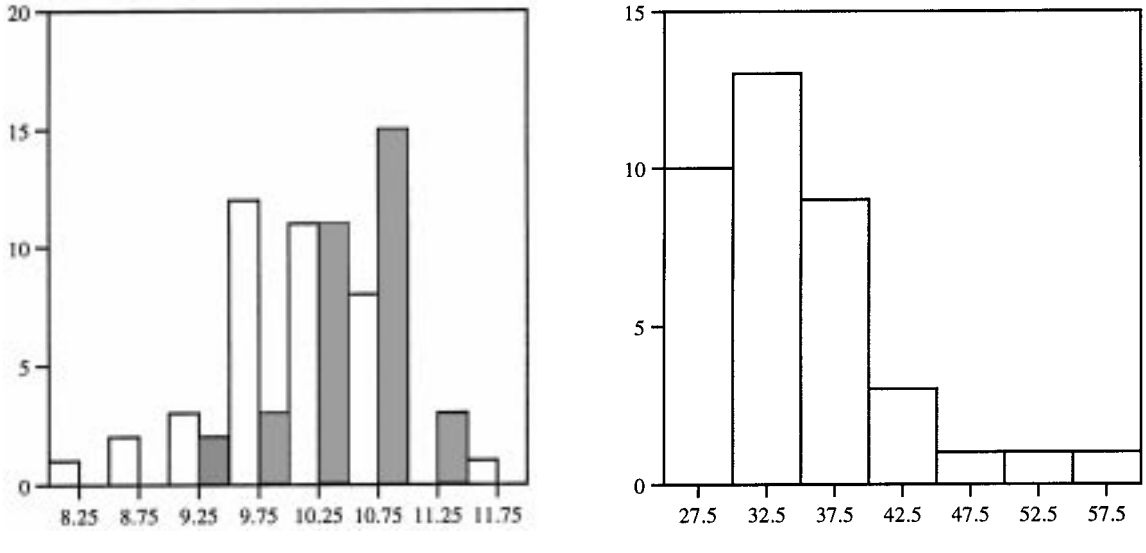


**Fig. 2. a)** Histogram of log($L_{\rm FIR}$) (in white) and log($L_B$) (in grey). **b)** Histogram of $T_{\rm FIR}$

**Table 2.** Blue and $H$-band magnitudes and far-infrared parameters

| Galaxy name | $B_{\rm T}^0$ | $m_{\rm H}$ | $f_{12.5}$ Jy | $f_{25}$ Jy | $f_{60}$ Jy | $f_{100}$ Jy | $T_{\rm FIR}$ K | $\log(L_{\rm FIR})$ $L_\odot$ |
|---|---|---|---|---|---|---|---|---|
| JB01 | 13.83 | 11.70 | | | | | | |
| JB02 | | 11.08 | | | | | | |
| JB03 | 14.41 | | <1.006E-01 | 8.518E-02 | 6.562E-01 | 1.414 | 35.0 | 10.33 |
| JB04 | 14.16 | 11.04 | | | | | | |
| JB05 | 13.72 | 11.34 | 1.754E-01 | 7.347E-01 | 2.980 | 2.852 | 52.4 | 10.38 |
| JB06 | | | 2.129E-01 | 4.172E-01 | 1.476 | 2.822 | 36.8 | 9.75 |
| JB07 | 15.31 | 11.01 | 3.032E-01 | 1.864 | 7.840 | 1.171E+01 | 41.5 | 10.96 |
| JB08 | 14.40 | 11.68 | <8.797E-02 | 1.115E-01 | 5.376E-01 | 1.386 | 32.7 | 9.93 |
| JB09 | 14.16 | 11.59 | | | | | | |
| JB10_1 | 13.34 | 13.09 | | | | | | |
| JB10_2 | | | | | | | | |
| JB11 | 14.00 | 11.92 | <1.898E-01 | 3.664E-01 | 2.818 | 6.650 | 33.9 | 10.76 |
| JB12_1 | | 10.97 | | | | | | |
| JB13 | 13.44 | 11.86 | <8.519E-02 | <1.784E-01 | 6.520E-01 | 2.089 | 29.8 | 9.89 |
| JB14 | | 11.69 | 1.398E-01 | 3.808E-01 | 3.909 | 7.289 | 37.2 | 11.16 |
| JB15 | | | <8.799E-02 | 9.234E-02 | 6.946E-01 | 2.341 | 29.4 | 10.34 |
| JB16 | 13.62 | 11.67 | <1.438E-01 | 1.383E-01 | 1.009 | 3.574 | 29.0 | 10.69 |
| JB17 | 12.11 | 11.75 | 1.238E-01 | 2.545E-01 | 3.250 | 6.391 | 36.4 | 8.87 |
| JB18 | 14.34 | 11.25 | <5.666E-02 | <4.950E-02 | 1.795E-01 | 5.924E-01 | 29.6 | 9.78 |
| JB19 | 12.98 | 13.00 | 7.142E-02 | 6.707E-02 | 4.746E-01 | 1.649 | 29.2 | 8.67 |
| JB20 | 14.07 | 10.81 | <6.290E-02 | <6.736E-02 | 1.610E-01 | <8.516E-01 | >26.0 | <9.24 |
| JB21 | | 13.21 | <5.883E-02 | <6.010E-02 | 3.101E-01 | 8.675E-01 | 31.5 | 9.15 |
| JB22 | | 12.68 | <4.014E-01 | <1.664E-01 | 6.994E-01 | 1.850 | 32.4 | 9.93 |
| JB23 | 14.47 | | <8.357E-02 | <6.012E-02 | 2.753E-01 | 1.112 | 27.8 | 10.12 |
| JB24 | 13.54 | 12.19 | <8.117E-02 | 6.942E-02 | 6.955E-01 | 1.276 | 37.6 | 8.46 |
| JB25 | | 12.07 | <1.524E-01 | <2.235E-01 | 4.593E-01 | 6.668E-01 | 42.0 | 10.41 |
| JB26 | | 13.17 | <7.811E-02 | 1.481E-01 | 1.203 | 2.818 | 33.9 | 10.67 |
| JB27 | 12.81 | 9.72 | <1.349E-01 | <1.814E-01 | 1.202 | 2.837 | 33.9 | 9.57 |
| JB28_1 | 11.35 | 10.04 | 1.320E-01 | 1.648E-01 | 1.666 | 6.613 | 28.0 | 10.15 |
| JB28_2 | 14.17 | | | | | | | |
| JB29 | 13.16 | 10.37 | <1.409E-01 | <1.442E-01 | 4.241E-01 | 1.074 | 33.0 | 9.57 |
| JB30 | | 11.25 | | | | | | |
| JB31 | | 12.80 | <5.612E-02 | <1.423E-01 | 4.616E-01 | 1.342 | 31.2 | 9.65 |
| JB32 | | 11.86 | <1.109E-01 | <7.854E-02 | 4.249E-01 | 1.464 | 29.2 | 9.03 |
| JB33 | 14.19 | 11.77 | | | | | | |
| JB34 | 13.59 | 11.54 | 1.645E-01 | 2.332E-01 | 2.444 | 5.231 | 35.1 | 10.79 |
| JB35 | | | | | | | | |
| JB36 | | 11.95 | 9.471E-02 | 4.593E-01 | 4.337 | 5.248 | 46.2 | 10.91 |
| JB37 | 13.20 | | 1.189E-01 | 2.719E-01 | 1.308 | 1.858 | 42.5 | 10.07 |
| JB38 | | | <1.011E-01 | 1.348E-01 | 1.038 | 2.471 | 33.6 | 10.73 |
| JB39 | 14.12 | 11.16 | <1.163E-01 | 1.419E-01 | 4.749E-01 | 1.956 | 27.8 | 9.97 |
| JB40 | | 12.18 | 2.844E-01 | 1.906 | 1.278E+01 | 9.948 | 58.9 | 11.62 |

at 60 $\mu$m only. It is interesting to note that all galaxies but two have fluxes at 60 and 100 $\mu$m lower than 5 and 8 Jy respectively. In that respect, our sample differs from most of the existing CO surveys of galaxies, in particular from the most extensive one, the FCRAO Extragalactic Survey carried out by Young et al. (1995) for which the galaxies satisfy at least one of the following criteria: (1) $B_{\rm T}^0 < 13$, (2) $f_{60} > 5$ Jy, or (3) $f_{100} > 10$ Jy. Only seven galaxies of our sample meet the FCRAO selection criterion. The two objects of our sample with highest far-infrared fluxes are the mergers JB07 and JB40. They are the most luminous FIR sources of the sample (9.1 $10^{10}$ and 4.2 $10^{11}$ $L_\odot$); they also have the highest $L_{\rm FIR}/L_B$ ratios. Their blue luminosities, however, are not exceptionally high: $10^{10}$ and

**Table 2.** continued

| Galaxy name | $B_T^0$ | $m_H$ | $f_{12.5}$ Jy | $f_{25}$ Jy | $f_{60}$ Jy | $f_{100}$ Jy | $T_{FIR}$ K | $\log(L_{FIR})$ $L_\odot$ |
|---|---|---|---|---|---|---|---|---|
| JB41 | 13.02 | 12.14 | <8.513E-02 | <2.142E-01 | 1.188 | 2.620 | 34.8 | 9.44 |
| JB42 | | 11.84 | | | | | | |
| JB43_1 | | | | | | | | |
| JB43_2 | | | | | | | | |
| JB44 | | 11.87 | <1.172E-01 | <1.30E-01 | 3.587E-01 | <1.725 | >26.4 | <10.18 |
| JB45 | 14.55 | | <1.179E-01 | 8.683E-02 | 1.138 | 2.850 | 33.0 | 9.99 |
| JB46 | | 12.41 | | | | | | |
| JB47 | | 13.08 | | | | | | |
| JB48 | | | 9.560E-02 | 2.805E-01 | 2.566 | 4.244 | 39.2 | 10.67 |
| JB49 | | 12.14 | <5.958E-02 | <1.327E-01 | 3.455E-01 | 1.152 | 29.6 | 10.18 |
| JB50 | | 10.81 | 2.143E-01 | 3.987E-01 | 3.660 | 6.842 | 37.2 | 10.02 |
| JB51 | | | <9.808E-02 | <1.402E-01 | 5.846E-01 | 1.448 | 33.3 | 10.07 |
| JB52 | 12.05 | | | | | | | |
| JB52_1 | | 10.18 | | | | | | |
| JB52_2 | | 9.78 | | | | | | |
| JB53 | 13.36 | 11.45 | 1.811E-01 | 4.368E-01 | 2.931 | 5.505 | 37.2 | 9.86 |
| JB54 | | 12.08 | <5.935E-02 | <9.806E-02 | 1.865E-01 | <7.504E-01 | >28.0 | <10.26 |
| JB55 | 13.11 | 12.44 | 9.859E-02 | 1.352E-01 | 1.392 | 4.026 | 31.2 | 9.69 |
| JB56 | 12.42 | 9.91 | | | | | | |
| JB57 | 13.94 | 11.96 | | | | | | |
| JB58 | 13.69 | 12.16 | | | | | | |
| JB59 | 14.60 | 11.67 | | | | | | |

$5\ 10^{10}\ L_\odot$. Figure 2a shows histograms of the FIR and blue luminosities $L_{FIR}$ and $L_B$. Figure 2b shows an histogram of the far-infrared temperatures $T_{FIR}$.

*Optical and near-infrared photometry and images:* Images presented in BJ95 show that star-formation is often distributed across the disks of the galaxies.

*Optical spectroscopy:* Optical spectra presented in BJ95 arise from the central $3'' \times 3''$ region of the sample galaxies. Few emission lines are visible in the spectra, suggesting that star-formation is not significanly enhanced in the central area. This has to be confirmed in a quantitative analysis.

## 4. Observations of the neutral gas and data reduction

The HI observations were carried out with a large beam that embraces the emission from the whole interacting system. In most cases, the beam of the CO observations is sufficiently small to separate the individual galaxies in an interacting system but large enough to encompass the whole CO emitting area of each galaxy.

### *4.1. The HI data*

The observations were made with the 64 m Parkes antenna in August 1994 and June 1995, and with the Australia Telescope Compact Array (ATCA) in March 1996. The Parkes radiotelescope has a beamwidth of $15'$ at $\lambda 21$ cm, a sensitivity of 0.63 K $Jy^{-1}$, and was equipped with a cryogenically cooled receiver with a system temperature of about 40 K for each linear polarization. The backend was a 2048 channel autocorrelator, with a bandwidth of 16 MHz. The galaxies were observed by position-switching between source and empty sky. The reference position was taken $5'$ time away from the source in right ascension. The data were reduced using the Spectral Line Analysis Package (SLAP). The spectra were smoothed to a final resolution of 6.6 km $s^{-1}$. The plots were made using the CLASS package (Forveille et al. 1990).

In some velocity intervals the Parkes observations were dominated by interference and these observations were repeated using the ATCA. The ATCA was used in its most compact configuration (array length of 122 m) since we were interesting in obtaining global HI spectra and not maps to be as closely consistent with the Parkes observations as possible. The synthesized beam of the ATCA was $5'$, the primary beam $33'$. The five antennas were fitted with cooled FET receivers. The backend was a 2048

channel autocorrelator, with a bandwidth of 8 MHz. PKS B1934-638 was used as a primary amplitude calibrator and for bandpass calibration and was observed every day. A secondary calibrator to correct for changes in gain and phase was observed at least once per hour. The data reduction was done using AIPS. The uv-data have been edited and calibrated, and global HI spectra were obtained using the command POSSM. The resolution of the ATCA spectra is 6.6 km s$^{-1}$. The final plots were made using CLASS and GRAPHIC.

### *4.2. The CO data*

The $^{12}$CO(1−0) observations have been carried out between June and December 1995 in La Silla (Chile) with the 15 m Swedish-ESO Submillimeter Telescope (SEST) (Booth et al. 1989). At 115 GHz, the telescope half-power beamwith is 43″. The main beam efficiency of SEST is $\eta_{\rm mb} = T_{\rm A}^*/T_{\rm mb} = 0.70$ (SEST handbook, ESO). We used a SIS receiver in single-sideband mode with $T_{\rm rec} \simeq 160$ K. During the observations, the typical system temperature was 300 K. A balanced on-off dual beam switching mode was used, with a frequency of 6 Hz and two symmetric reference positions offset by 12′ in azimuth. The pointing was regularly checked on nearby SiO masers. The pointing uncertainties were about 5″. The backend was a 1600 channel low-resolution acousto-optical spectrometer with a total bandwith of 1 GHz, which provided at 115 GHz a velocity resolution of 1.8 km s$^{-1}$. The data were reduced using the software CLASS. The spectra were smoothed to a final velocity resolution of 14.6 km s$^{-1}$. Only first order baselines were subtracted from the spectra.

The uncertainties in the integrated CO and HI line intensities have been computed on the following way: they are the quadratic sum of errors due to noise in the spectrum and in the determination of the baseline:

$$\Delta I = \sigma_{\rm rms}\, \Delta v_{\rm i}\, ([\Delta v_{\rm c}/\Delta v_{\rm i}]^{1/2} + [\Delta v_{\rm c}/\Delta v_{\rm b}]^{1/2}) \quad (1)$$

where $\Delta v_{\rm i}$ = velocity range over which the spectrum was integrated, $\Delta v_{\rm c}$ = the smoothed channel width (14.6 km s$^{-1}$ for the CO spectra and 6.6 km s$^{-1}$ for the HI spectra) and $\Delta v_{\rm b}$ = the velocity range over which the baseline was fitted.

### *4.3. Atomic and molecular gas masses*

The HI masses are related to the HI integrated intensities $F$(HI) (in Jy km s$^{-1}$) by:

$$M({\rm HI})\,(M_\odot) = 2.36\,10^5\, F({\rm HI})\,(D/1\ {\rm Mpc})^2 \quad (2)$$

where $D$ is the distance to the galaxy in Mpc.

For the conversion factor from CO emissivities into $H_2$ column densities, we use the value of Strong et al. (1988):

$$N({\rm H_2})/I_{\rm mb}({\rm CO}) = 2.3\,10^{20}\,{\rm mol\,cm^{-2}}\,({\rm K\ km\ s^{-1}})^{-1} \quad (3)$$

where $I_{\rm mb}({\rm CO}) = \int T_{\rm mb} {\rm d}v$ is the main-beam line area. For the SEST 43″ beam, this converts into

$$M({\rm H_2})\,(M_\odot) = 1.25\,10^5\, I_{\rm mb}({\rm CO})\,(D/1\ {\rm Mpc})^2. \quad (4)$$

The conversion factor $X$ has been established empirically for our own galaxy and may differ for other galaxies (for a discussion about the conversion factor, see e.g. Lequeux 1995). Recent studies have reopened the question of the use of the CO emission as a star-formation indicator: although stars form in the dense cores of molecular clouds, it turns out that on galaxy scale, some observations have shown that HI masses are better correlated with other star-formation indicators (UV, H$\alpha$) than CO luminosities (e.g., Kennicutt 1989; Buat 1992; Casoli et al. 1996). For luminous objects however, a positive correlation has been found between the molecular gas content (as derived from CO line intensities using a standard conversion factor $X$) and star-formation activity (as traced by the H$\alpha$ equivalent width and the far-infrared emission) (Boselli et al. 1995). This suggests that the value of $X$ may vary from one galaxy to another; for the low-luminosity ones which are less metal-rich, $H_2$ masses may be underestimated by using a standard conversion factor. The $H_2$ masses we have computed thus have to be taken as *estimates* of the molecular hydrogen masses. The value we adopted for $X$ has been choosen to be consistent with previous papers and allow direct comparison with other samples.

## 5. Observational biases due to limited telescope sensitivity

Many of the sample objects are rather distant and have weak far-infrared fluxes (see Sect. 3). The detection limit of the IRAS satellite ($f_{60} \approx 0.2$ and $f_{100} \approx 0.8$ Jy) implies that at radial velocities larger than 10000 km s$^{-1}$, only galaxies with a FIR luminosity higher than $10^{10}\ L_\odot$ could be detected by IRAS.

Similarly, an observational bias was introduced in the CO and HI data, the choice of a reasonable integration time setting a limit to the HI and $H_2$ gas masses which could be detected. On the average, an integration time of 4 hours has been spent on each galaxy, which corresponds to a noise level of about 3 mK (in $T_{\rm A}^*$) in the CO data and 3 mJy in the HI data for the velocity resolutions of our spectra. An upper limit to the emission can be determined as $I = \sigma\,\Delta v$. Using a linewidth $\Delta v$=150 km s$^{-1}$. this means that within 4 hours of integration a limit of $10^9\ M_\odot$ ($10^8\ M_\odot$ respectively) on the $H_2$ mass is reached only for galaxies with $v < 8000$ km s$^{-1}$ ($v < 2800$ km s$^{-1}$ respectively). For HI, a limit of $10^9\ M_\odot$ is reached within 4 hours for galaxies with $v < 7300$ km s$^{-1}$.

## 6. Global results of the HI and CO observations

The HI and CO spectra are shown in Fig. 3 for a few galaxies of the sample. The entire dataset is presented in

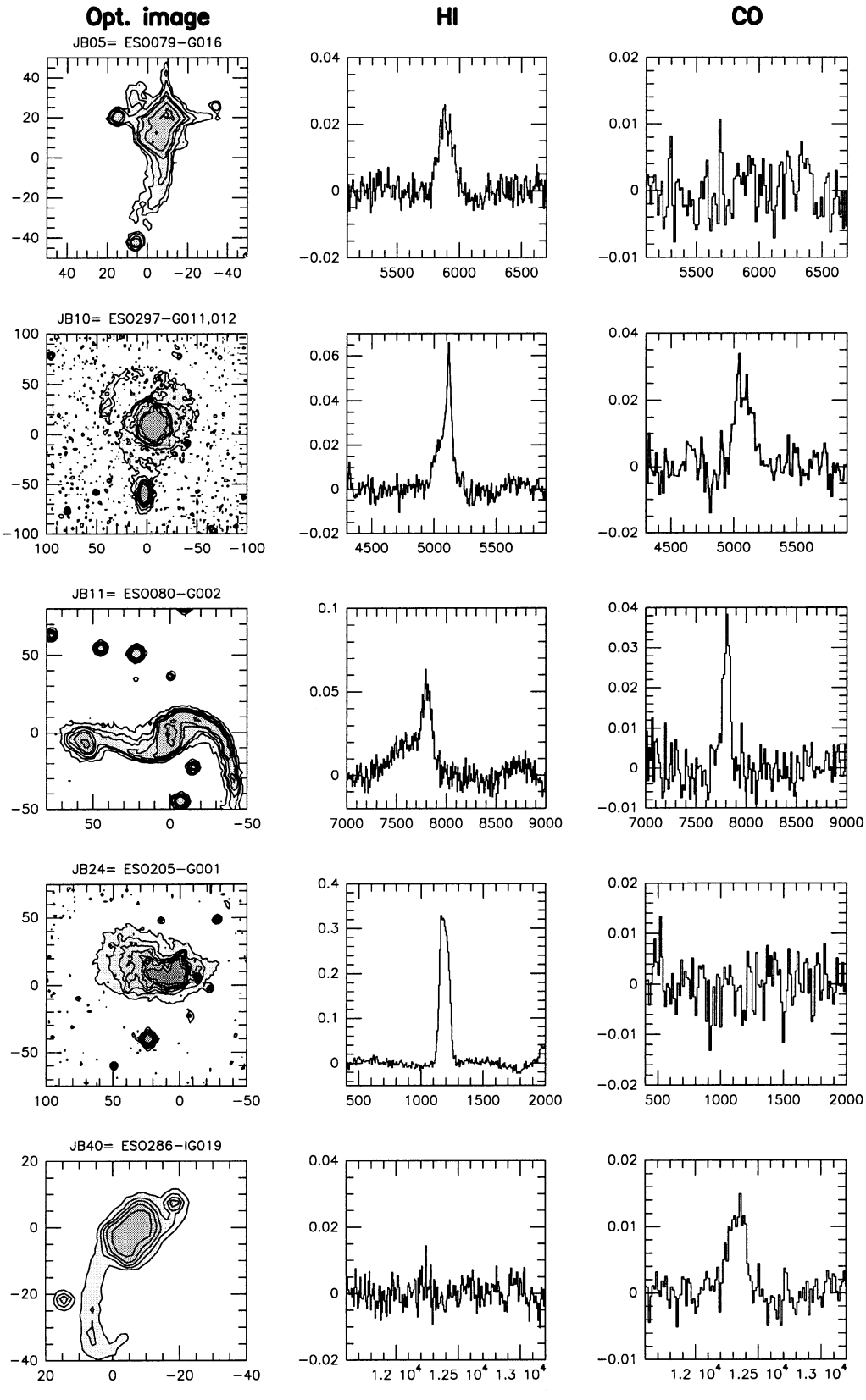


**Fig. 3.** Optical images, HI and CO spectra for a few galaxies of the sample. The entire dataset is presented in the electronic version of the paper. **Column 1**: contour and grey-scale pictures of the galaxies (ESO Digitized Sky Survey). North is to the top, west to the right. The scales on the axes are in arcsec. **Column 2**: HI spectra. The spectral resolution is 6.6 km s$^{-1}$. The units are km s$^{-1}$ on the $X$ axis (radial velocities in the radio convention) and Jy on the $Y$ axis. **Column 3**: CO spectra. The spectral resolution is 14.6 km s$^{-1}$. The units are km s$^{-1}$ on the $X$ axis (radial velocities in the radio convention) and $K$ on the $Y$ axis ($T_{\rm A}^{*}$)

**Table 3.** HI and CO, observational results

| Name | $v_{\rm HI}$ [kms$^{-1}$] | $\Delta v_{\rm HI}$ [kms$^{-1}$] | $\int S_{\rm HI} {\rm d}v$ [Jy km s$^{-1}$] | $M$(HI) [$10^9$ $M_\odot$] | Instrument used | Name | $v_{\rm CO}$ [kms$^{-1}$] | $\Delta v_{\rm CO}$ [kms$^{-1}$ | $\int T_{\rm A}^*({\rm CO}) {\rm d}v$ [K km s$^{-1}$] | $M(H_2)$ [$10^8$ $M_\odot$] | |
|---|---|---|---|---|---|---|---|---|---|---|---|
| JB01 | N.O. | | | | | JB01 | | | <0.4 | <11.4 | * |
| JB02 | N.O. | | | | | JB02 | | | <0.4 | <12.3 | |
| JB03 | | | <0.6 | <2.7 | ATCA | JB03_2 | | | <0.3 | <10.0 | |
| JB04 | | | <1.2 | <2.4 | ATCA | JB04 | | | <0.6 | <9.1 | |
| JB05 | 5890 | 355 | 2.9±0.2 | 4.2 | Parkes | JB05 | | | <0.5 | <5.5 | |
| JB06 | | | <1.0 | <0.5 | Parkes | JB06_1 | | | <0.5 | <2.0 | |
| JB07 | 6557 | 540 | 5.2±0.3 | 9.4 | Parkes | JB07 | 6602 | 469 | 4.7±0.5 | 65.0 | |
| JB08 | | | <1.0 | <1.9 | Parkes | JB08 | | | <0.3 | <4.5 | |
| JB09 | | | <0.9 | <2.2 | Parkes | JB09 | | | <0.3 | <5.2 | |
| JB10 | 5092 | 354 | 5.8±0.3 | 6.3 | Parkes | JB10_1 | 5082 | 303 | 4.1±0.5 | 33.6 | |
| JB11[(a)] | 7738 | 717 | 12.2±0.6 | 30.6 | Parkes | JB11_1 | 7806 | 274 | 3.2±0.4 | 61.9 | |
| JB12 | | | <1.0 | <1.6 | ATCA | JB12_1 | | | <0.3 | <3.6 | |
| | | | | | | JB12_2 | | | <0.3 | <3.6 | |
| JB13 | 5628 | 523 | 15.0±0.4 | 20.0 | Parkes | JB13 | | | <0.4 | <4.0 | |
| JB14 | N.O. | | | | | JB14_2 | | | <0.3 | <12.3 | |
| JB15 | 9111 | 531 | 6.8±0.3 | 23.8 | Parkes | JB15 | 9161 | 475 | 1.7±0.3 | 45.3 | |
| JB16 | | | <1.2 | <6.0 | ATCA | JB16 | 11159 | 553 | 3.6±0.3 | 142.3 | |
| JB17 | 863 | 293 | 43.9±0.4 | 1.4 | ATCA | JB17_1 | 847 | 218 | 0.45±0.15 | 0.1 | |
| JB18 | | | <0.6 | <2.0 | ATCA | JB18 | | | <0.5 | <13.0 | |
| JB19 | 1327 | 197 | 1.4±0.3 | 0.1 | ATCA | JB19 | | | <1.2 | <0.7 | |
| JB20 | | | <0.5 | <0.4 | ATCA | JB20 | | | <0.5 | <3.1 | |
| JB21 | 3816 | 303 | 3.2±0.2 | 2.0 | Parkes | JB21 | | | <0.5 | <2.3 | |
| JB22 | 6126 | 287 | 1.9±0.2 | 3.0 | Parkes | JB22 | 6114 | 455 | 7.7±1.0 | 91.4 | |
| JB23 | 10863 | 354 | 7.0±0.1 | 34.7 | Parkes | JB23 | | | <0.7 | <26.2 | |
| JB24 | 1188 | 186 | 29.3±0.1 | 1.7 | Parkes | JB24 | | | <0.7 | <0.3 | |
| JB25 | N.O. | | | | | JB25 | | | <0.4 | <26.7 | |
| JB26 | | | <0.8 | <4.0 | ATCA | JB26 | | | <0.3 | <11.5 | |
| JB27 | | | <0.8 | <0.3 | Parkes | JB27 | | | <0.7 | <2.1 | |
| JB28 | 4644 | 942 | 20.1±0.5 | 18.2 | Parkes | JB28_1 | 4814 | 280 | 1.3±0.3 | 9.6 | |
| JB29 | | | <0.9 | <1.0 | Parkes | JB29_1 | | | <0.6 | <5.2 | * |
| JB30 | | | <1.5 | <1.7 | ATCA | JB30 | | | <0.8 | <7.0 | |
| JB31 | 5130 | 370 | 5.8±0.4 | 6.4 | Parkes | JB31 | | | <1.7 | <14.2 | |
| JB32 | 2515 | 253 | 7.7±0.3 | 2.0 | Parkes | JB32 | | | <0.8 | <1.6 | |
| JB33 | N.O. | | | | | JB33 | | | <0.5 | <39.5 | |
| JB34 | 8939 | 356 | 4.6±0.3 | 15.4 | ATCA | JB34 | | | <0.8 | <20.3 | |
| JB35 | N.O. | | | | | JB35 | N.O. | | | | |
| JB36 | | | <0.7 | <2.2 | ATCA | JB36 | | | <0.6 | <14.5 | |
| JB37 | 5976 | 280 | 2.6±0.4 | 3.9 | ATCA | JB37 | 5884 | 350 | 1.6±0.3 | 17.6 | |
| JB38 | 12606 | 645 | 3.0±0.3 | 20.0 | Parkes | JB38_1 | | | <0.3 | <15.1 | |
| | | | | | | JB38_2 | | | <0.5 | <25.2 | |
| JB39 | | | <1.0 | <1.9 | ATCA | JB39_1 | | | <0.4 | <5.8 | |
| | | | | | | JB39_2 | | | <0.8 | <11.6 | |
| JB40 | | | <0.5 | <3.5 | Parkes | JB40 | 12331 | 287 | 2.0±0.2 | 96.5 | |
| JB41 | 2609 | 355 | 13.6±0.5 | 3.9 | Parkes | JB41 | | | <0.5 | <1.1 | |
| JB42 | N.O. | | | | | JB42 | | | <0.4 | <9.0 | |
| JB43 | 8928 | 421 | 1.6±0.2 | 5.4 | Parkes | JB43_1 | | | <0.6 | <15.2 | |
| | | | | | | JB43_2 | 8865 | 211 | 0.8±0.3 | 20.0 | |
| JB44 | 9254 | 220 | 1.8±0.3 | 6.5 | ATCA | JB44 | | | <0.5 | <13.6 | |
| JB45 | 5086 | 390 | 2.5±0.5 | 2.7 | ATCA | JB45_1 | | | <0.6 | <4.9 | |
| | | | | | | JB45_2 | | | <0.6 | <4.9 | |
| JB46 | N.O. | | | | | JB46_1 | | | <0.7 | <77.3 | |
| | | | | | | JB46_2 | | | <0.5 | <55.2 | |
| JB47 | N.O. | | | | | JB47_1 | | | <0.5 | <9.7 | |
| | | | | | | JB47_2 | | | <0.6 | <11.7 | |

**Table 3.** continued

| Name | $v_{\rm HI}$ [km s$^{-1}$] | $\Delta v_{\rm HI}$ [km s$^{-1}$] | $\int S_{\rm HI}{\rm d}v$ [Jy km s$^{-1}$] | $M$(HI) [$10^9$ $M_\odot$] | Instrument used | Name | $v_{\rm CO}$ [km s$^{-1}$] | $\Delta v_{\rm CO}$ [km s$^{-1}$ | $\int T_{\rm A}^*({\rm CO}){\rm d}v$ [K km s$^{-1}$] | $M$(H$_2$) [$10^8$ $M_\odot$] |
|---|---|---|---|---|---|---|---|---|---|---|
| JB48 | | | <0.9 | <2.5 | ATCA | JB48 | 8374 | 286 | 1.9±0.4 | 42.3 |
| JB49 | | | <0.7 | <3.5 | ATCA | JB49 | 10560 | 430 | 1.4±0.4 | 49.6 (tentative) |
| JB50 | 3039 | 320 | 5.9±0.4 | 2.3 | Parkes | JB50 | 3078 | 253 | 2.6±0.3 | 7.8 |
| JB51 | | | <0.8 | <1.9 | ATCA | JB51 | | | <0.4 | <7.8 |
| JB52 | | | <1.1 | <0.4 | Parkes | JB52_1 | | | <0.6 | <1.8 |
| JB53 | 2883 | 316 | 6.5±0.3 | 2.3 | Parkes | JB53 | 2869 | 358 | 1.9±0.4 | 5.0 |
| JB54 | N.O. | | | | | JB54 | | | <0.3 | <20.2 |
| JB55 | 3307 | 422 | 10.6±0.5 | 4.9 | Parkes | JB55 | 3334 | 236 | 1.6±0.3 | 5.6 |
| JB56 | 2718 | 633 | 3.7±0.3 | 1.2 | Parkes | JB56 | | | <0.5 | <1.2 |
| JB57,58 | | | <1.0 | <4.2 | ATCA | JB57 | | | <0.5 | <15.4 |
| JB58 | see JB57 | | | | | JB58 | 10121 | 684 | 3.3±0.2 | 107.3 |
| JB59 | | | <1.5 | <3.0 | ATCA | JB59 | | | <0.8 | <12.1 |

N.O.: Not observed.
∗: Galaxies with uncertain positions (30 × 30 arcsec).
(a) JB11: for the HI, the pointing was made toward the position between the two galaxies JB11_1 and JB11_2: 01h35m50.5; −65d09m02.

the electronic version of the paper. The results are listed in Table 3, arranged as follows:

- *Columns 1 and 7*: Galaxy number adapted from Johansson & Bergvall (1990). The HI data refer to the entire system; in some cases, the two galaxies have been observed in CO.

- *Columns 2 and 8*: Radial velocity (in the radio convention). For the detected galaxies, the centroid velocity of the HI and CO line is given. For the non-detected ones, the values have been taken from NED or given by Bergvall (private communication). N.O.= not observed.

- *Columns 3 and 9*: Linewidth at the base of the HI and CO profile.

- *Columns 4 and 10*: Integrated HI and CO line intensity.

- *Column 5*: HI mass.

- *Column 6*: Instrument used for the HI observations: ATCA (Australian Telescope Compact Array) or Parkes.

- *Column 11*: $H_2$ mass. The asterisk indicates the galaxies with uncertain positions (30 × 30 arcsec).

### 6.1. Individual cases

HI fluxes exist in the literature for two galaxies of the sample, JB17 and JB24 (Huchtmeier & Richter 1989). Our ATCA data give a lower value for the HI flux of JB17: $43.9 \pm 0.4$ against $53.9 \pm 4.8$ Jy km s$^{-1}$. In that galaxy, the HI might be distributed over an area which is larger than the 5″ synthesized beam and we might be underestimating the total flux. Our Parkes spectrum gives also a lower value for the flux of JB24: $29.3 \pm 0.1$ against $36 \pm 4$ Jy km s$^{-1}$. We cannot offer an explanation for this discrepancy of more than 10%.

Four galaxies of the sample have previously been observed in CO with SEST by other authors: the brightest far-infrared sources, JB07 and JB40, were included in the sample of luminous infrared southern galaxies observed by Mirabel et al. (1990); JB07, JB11 and JB58 belong to the sample of southern isolated pairs of galaxies observed by Combes et al. (1994). All spectra agree within the error bars except for JB11 for which we measured an integrated CO intensity $\int T_{\rm A}^*{\rm d}v$ of $3.2 \pm 0.4$ K km s$^{-1}$ and Combes et al. 2.4. This difference probably comes from the fact that we have set a wider window because our spectrum looks slightly broader at the base.

### 6.2. Detection rate in HI and $^{12}$CO(1−0)

Out of 48 galaxies observed in HI, 26 were detected, which coresponds to a detection rate of 54%. The 57 interacting systems listed by JB90 for which information on radial velocity is available were observed in CO. In some cases, the two galaxies in a pair were observed. In total, spectra were obtained for 65 galaxies, out of which 16 were clearly detected, 1 tentatively (detection rate of 26%).

### 6.3. HI and $H_2$ masses

Figure 4 shows the values of the HI and $H_2$ masses versus $H$-band luminosity for all observed galaxies for which $H$-band magnitudes are available (see Table 2). The $H$-band luminosities have been computed using

$L_{\rm H}/L_\odot = (D/1\ {\rm Mpc})^2\, 10^{11.36-m_{\rm H}/2.5}$. It appears clearly that on the average, the galaxies have an HI mass that is significantly higher than their $H_2$ mass. If we consider the systems for which both HI and CO have been detected (12 systems), we find $\log(M({\rm HI})/M(H_2)) = 0.62 \pm 0.43 = \log(4.2)$. If we take all the galaxies detected in HI (26 systems), we get $\log(M({\rm HI})/M(H_2)) > 0.80 \pm 0.33 = \log(6.3)$, which means that these galaxies have less than 15% of their gas in molecular form. A similar result has been found for the nearby cluster Fornax (Horellou et al. 1995) and differs from results obtained for samples selected on their far-infrared emission which seem to have a much higher fraction of their gas in molecular form.

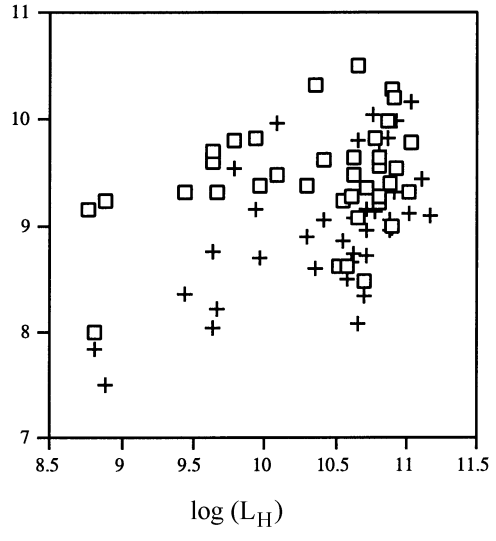


**Fig. 4.** HI (squares) and $H_2$ (crosses) masses versus $H$-band luminosity $L_{\rm H}$ (all in logarithmic scale)

*Acknowledgements.* We wish to thank the staffs at SEST, Parkes and Narrabri for the help during the observations. Thank you to Susanne Aalto-Bergman for her interest in the project, to Tommy Wiklind for having carried out some of the CO observations, to Jim Higdon and Bärbel Koribalski for their advice during the reduction of the interferometer data, to Nils Bergvall for stimulating discussions, to Bill Cast for encouraging comments. We thank the referee, Alessandro Boselli, for careful reading of the manuscript and useful suggestions. The Australia Telescope is funded by the Commonwealth of Australia for operation as a National Facility managed by CSIRO. This research has made use of the NASA/IPAC Extragalactic Database (NED) which is operated by the Jet Propulsion Laboratory, Caltech, under contract with the National Aeronautics and Space Administration. The optical images have been retrieved from the Digitized Sky Survey. The Digitized Sky Survey (DSS) was produced by the Space Telescope Science Institute (STScI) and is based on photographic data from the UK Schmidt Telescope, the Royal Observatory Edinburgh, the UK Science and Engineering Research Council, and the Anglo-Australian Observatory.

## References

Bergvall N., 1981, Uppsala Obs. Rep. 19, (B81)
Bergvall N., Johansson L., 1995, A&AS 113, 499 (BJ95)
Booth R.S., Delgado G., Hagström M., et al., 1989, A&A 216, 315
Boselli A., Gavazzi G., Lequeux J., et al., 1995, A&A 300, L13
Braine J., Combes F., 1993, A&A 269, 7
Buat V., 1992, A&A 264, 444
Casoli F., Dickey J., Kazès, I., et al., 1996, A&A 309, 43
Combes F., Prugniel P., Rampazzo R., Sulentic J.W., 1994, A&A 281, 725
Forveille T., Guilloteau S., Lucas R., 1990, IRAM internal report (CLASS)
Horellou C., Casoli F., Dupraz C., 1995, A&A 303, 361
Huchtmeier W.K., Richter O.G., 1989, A General Catalog of HI Observations of Galaxies. Springer-Verlag
Hummel E., van der Hulst J.M., Kennicutt R.C., Keel W.C., 1990, A&A 236, 333
Johansson L., Bergvall N., 1990, A&AS 86, 167 (JB90)
Kennicutt R.C., Roettiger K.A., Keel W.C., van der Hulst J.M., Hummel E., 1987, AJ 93, 1011
Kennicutt R., 1989, ApJ 344, 685
Lequeux J., 1995, in "The interplay between massive star-formation, the interstellar medium and galaxy evolution", Kunth et al. (ed.). Frontières, p. 105
Lonsdale C.J., Helou G., Good J.C., Rice W., 1985, Catalogued galaxies and quasars observed in the IRAS survey, Jet Propulsion Laboratory
Martin J.-M., Bottinelli L., Gouguenheim L., Dennefeld M., 1991, A&A 245, 393
Mirabel F., Booth R.S., Garay G., Johansson L.E.B., Sanders D.B., 1990, A&A 236, 327
Strong A.W., Bloemen J.B.G.M., Dame T.M., et al., 1988, A&A 207, 1
Vaucouleurs de G., Vaucouleurs de A., Corwin H.G., et al., 1991, Third Reference Catalogue of Bright Galaxies. Springer-Verlag (RC3)
Xu G., Sulentic J.W., 1991, ApJ 374, 407
Young J., Shuding Xie, Tacconi L., et al., 1995, ApJS 98, 219